Effect of Multielectronic Configurations on the XAFS Analysis at the Fe K Edge

Paola D'Angelo*,† and Maurizio Benfatto‡

Dipartimento di Chimica, Università di Roma "La Sapienza", P. le A. Moro 5, 00185 Roma, Italy, INFM, UdR Camerino, Italy, and Laboratori Nazionali di Frascati, INFN, P.O. Box 13, 00044 Frascati, Italy

Received: January 2, 2004; In Final Form: March 15, 2004

An extensive investigation of the extended X-ray absorption fine structure (EXAFS) spectra of Fe^{2+} and Fe^{3+} in aqueous solution is presented. Anomalous peaks at 3.9 and 5.3 $Å^{-1}$ have been detected and assigned to the simultaneous excitations of the 1s3p and 1s3s electrons, referred to as KM_{23} and KM_1 channels. The Fe^{3+} water solution absorption cross section displays the presence of peculiar features that reflect the existence of two electronic configurations in the ground state, giving rise to two channels of comparable intensity. The influence of many-body effects on the quantitative extraction of the structural parameters from the EXAFS spectra was investigated. Omission of double-electron excitation edges from the atomic background significantly worsens the quality of the EXAFS fits and results in slightly incorrect values of the structural parameters. Conversely, the $[Fe(H_2O)_6]^{3+}$ structural parameters obtained from the EXAFS data analysis, performed in the framework of the one-electron approximation, are affected by severe systematic errors, despite the perfect agreement between the experimental and theoretical data. An accurate determination of the hydration geometry of the Fe^{3+} ion can be only obtained using a theoretical scheme based on the multichannel multiple-scattering theory. The hydrogen contribution has been included in the EXAFS data analyses and Fe−H distances of 2.84 and 2.76 Å have been obtained for Fe^{2+} and Fe^{3+}, respectively, which are in excellent agreement with the results of ab initio quantum-mechanical/molecular-mechanical molecular dynamics simulations.

1. Introduction

With the availability of intense third-generation synchrotron radiation sources, the past decade has seen a rebirth of interest in X-ray absorption spectroscopy (XAS), with a growing list of applications in a variety of scientific fields. Similarly, new theoretical advances in the calculation of X-ray absorption cross sections have considerably improved the reliability of theoretical standards,[1,2] and today the XAS technique can be considered one of the most powerful tools to obtain quantitative structural information on the local environment of an excited atom.

Even if valuable chemical and structural information have been obtained by XAS experiments on a large number of systems, some important points concerning the comparison between the experimental and calculated absorption cross sections have not, until now, been properly addressed. Several investigations on gaseous and condensed systems have shown the existence of multielectron photoexcitations superimposed onto the smooth energy dependence of the dominant channel of the single-electron photoeffect.[3−7] Moreover, the presence of peculiar features arising from two independent electronic configurations of the final state has been found in the X-ray absorption near edge (XANES) spectra of some compounds. This phenomenon has been detected at the Eu L_3 edge of homogeneous and inhomogeneous mixed-valent materials,[8] at the Cu K edge of Nd_2CuO_4 and La_2CuO_4 compounds,[9] and at the Fe K edge of $[Fe(H_2O)_6]^{3+}$ complexes in solution.[10] In these cases, the theoretical cross section calculated in the usual one-electron approximation within the multiple-scattering (MS) theory framework is not able to correctly reproduce the experimental data. In particular, the low-energy part of these XAS spectra shows the presence of features closely resembling the main structures associated with the fully relaxed electronic configuration that are not accounted for by the one-electron approximation. A description of this phenomenon was given some years ago, using a scheme that extends the one-electron multiple-scattering theory to cases where the ground state is a real many-body wave function accounting for different electronic channels.[11] This multichannel multiple-scattering (MCMS) theory can be a valid aid in interpreting XAS experimental data, although it has not been implemented in any computer code.

Until now, the problem of the influence of multichannel contributions on the extraction of the structural parameters from the XAS data has not been properly dealt with. These effects are likely to affect the parameters linked to the amplitude of the signal, such as the Debye−Waller (DW) factors and the coordination numbers.

The aim of this paper is to investigate the influence of many-body effects on the quantitative extraction of the structural parameters from the X-ray absorption fine structure (EXAFS) spectra. To this end, we will carry out an accurate XAS analysis of Fe^{2+} and Fe^{3+} aqueous solutions that are ideal systems, as the structural description of the hydration sphere of these ions has been provided by a variety of experimental and theoretical methods.[12] By properly accounting for the presence of multielectron configurations, it is possible to improve the reliability of the EXAFS analysis at the Fe K edge and to provide an accurate determination of the hydration properties of the Fe^{2+} and Fe^{3+} ions. The contrasting coordination of these cations is of significance in explaining fundamental aspects of electrochemical processes, and the redox reaction which couples these ions is one of the most fundamental in chemical kinetics. Clearly ferrous and ferric cations, and compounds of iron, are worthy of deep investigation because of their presence in many

† Università di Roma "La Sapienza" and INFM.
‡ Laboratori Nazionali di Frascati.

10.1021/jp0499732 CCC: $27.50
Published on Web 04/22/2004

commercially important processes, both as useful materials in chemical reactions and as unwanted products due to corrosion. Moreover, iron is one of the key elements in biology, and it plays an important role in the activity of large biomolecules in solutions. The results of this study provide the basis for the quantitative analysis of the XAS spectra at the Fe K edge.

2. Methods

2.1. Experimental Spectra. Fe K-edge X-ray absorption spectra of 100 mM Fe^{2+} and Fe^{3+} water solutions were recorded at the ESRF (Grenoble, France), beam-line BM29,[13] with ring energy 6 GeV and ring current 175 mA. Samples were prepared by dissolving $FeSO_4 \cdot 7H_2SO_4$ and $Fe_2(SO_4)_3$ in deionized water. The pH of the solutions was 2 and 4 for Fe^{2+} and Fe^{3+}, respectively, and was fixed by controlled addition of HNO_3. Spectra were recorded in transmission mode using a Si(311) double-crystal monochromator, detuned to 50% of the rocking curve full width at half-maximum, for harmonic rejection. The energy calibration was performed by recording the iron foil spectrum. Data points were collected for 1 s each, and several spectra were recorded and averaged. The solutions were kept in cells with Kapton film windows and Teflon spacers of 0.8 μm.

2.2. EXAFS Data Analysis. To extract structural information from the XAS spectra, we used an advanced theoretical scheme based on a multiple-scattering formalism. The data analysis was performed by means of the GNXAS code,[14,15] which is based on the calculation of the EXAFS signal and a subsequent refinement of the structural parameters. The GNXAS method accounts for MS paths, with correct treatment of the configurational average of all the MS signals to allow fitting of correlated distances and bond variances (Debye−Waller factors).

Recently, it has been shown that the inclusion of hydrogen atoms is essential to perform a quantitative analysis of the EXAFS spectra of 3d transition metal ions in water solution.[16] Here, the hydrogen atoms were included both in the potential and in the cross-section calculations. A correct description of the first hydration sphere of ionic solutions has to account for asymmetry in the distributions. Therefore, the Fe−O and Fe−H two-body theoretical signals associated with the first-shell water molecules were modeled with Γ-like distribution functions,[17,18] which depend on four parameters: the coordination number, N, the average distance, R, the mean-square variation, σ, and the skewness, β. Note that β is related to the third cumulant C_3 through the relation $C_3 = \sigma^3\beta$, and R is the first moment of the function $4\pi \int g(r)r^2\, dr$. It is important to stress that R is the average distance and not the position of the maximum of the peak (R_m). R is longer than R_m for asymmetric distributions, while these values are equal for peaks which result in Gaussian functions ($\beta = 0$). The first-shell water signals were calculated assuming an octahedral coordination of the water molecules around the Fe ions.

Several EXAFS analyses on 3d transition metal aqueous complexes pointed out the importance of accounting for MS effects within the first hydration shell.[16,19,20] The strongest MS contributions are generated by the three linear O−Fe−O configurations due to the well-known focusing effect, which enhances the amplitude of the three-body signals associated with linear configurations. Nevertheless, the MS signals associated with the 12 rectangular O−ion−O triangles provide a detectable contribution, and they have been included in the theoretical curve.

Phase shifts were calculated using muffin-tin potentials and advanced models for the exchange−correlation self-energy (Hedin−Lundqvist).[21] The values of the muffin-tin radii were 0.2, 0.9, and 1.2 Å for hydrogen, oxygen, and iron, respectively. The muffin-tin radius of the hydrogen atoms, which corresponds to about 0.06 electron for the integral of the charge density, was adjusted so as not to overestimate the signal from the scattering of hydrogen atoms, which is expected to be weak. Inelastic losses of the photoelectron in the final state were accounted for intrinsically by complex potential. The imaginary part also includes a constant factor accounting for the core-hole width (1.25 eV fwhm).[22]

The $\chi(k)$ theoretical signal is related to the experimental absorption coefficient $\alpha(k)$ through the relation:

$$\alpha(k) = J\sigma_0(k)[1 + S_0^2\chi(k)] + b(k) \quad (1)$$

where $\sigma_0(k)$ is the K-edge atomic cross section, J is the edge jump, S_0^2 provides a uniform reduction of the signal and is associated with the many-body corrections to the one-electron cross section, and $b(k)$ is the background due to further absorption processes. Double-electron excitations are accounted for by modeling the $b(k)$ function as the sum of a smooth polynomial spline plus a step-shaped function, as described in ref 23. Each function depends on three parameters, which represent the edge position relative to the single-hole state, E_d, the width, ΔE, and the jump, H, of the double-electron channel contribution. This background is then summed to the structural contribution to build a theoretical signal that is fitted to the raw data. It is well known that shake-up, shake-off, and resonant channels contribute to double-electron photoexcitations, and, while the onset of shake-up channels is quite sharp, shake-off and resonant channels show large onsets at the threshold. The step-shaped function used in our atomic background model provides a good description of the shake-up channels only. Nevertheless, this model function has been found to allow a reliable extraction of the structural parameters, which are not very sensitive to the fine details of the atomic background used in the EXAFS analysis.[7]

Least-squares fits are performed by minimizing a residual function of the type:

$$R_{sq}(\{\lambda\}) = \sum_{i=1}^{N} \frac{[\alpha_{exp}(E_i) - \alpha_{mod}(E_i; \lambda_1, \lambda_2, ..., \lambda_p)]^2}{\sigma_i^2} \quad (2)$$

where N is the number of experimental points, $E_i,\{\lambda\} = (\lambda_1, \lambda_2, ..., \lambda_p)$ are the p parameters to be refined, and σ_i^2 is the variance associated with each experimental point, $\alpha_{exp}(E_i)$. In most cases, σ_i^2 can be directly estimated from the experimental spectrum and a k^m weighting (with $m = 2, 3, ...$) results in a good approximation.[15,23]

The refinement of EXAFS spectra was performed using the following structural parameters: the Fe−O and Fe−H first-shell average distance, R, variance, σ^2, and skewness, β; the angle, θ, angle variance, σ_θ^2, bond−bond, ρ_{R1R2}, and bond−angle, $\rho_{R1\theta}$, dimensionless correlations for each 90° configuration; the angle variance, σ_θ^2, and bond−bond, ρ_{R1R2}, correlation for each 180° configuration. The 180° angles were kept fixed at their equilibrium extremal values. Details about this parametrization of the three-body configurations can be found in ref 15. Other important nonstructural parameters included in the refinement were the energy difference between the experimental and theoretical scale and the amplitude correction factor S_0^2.

3. Results

3.1. Experimental Evidence of Multielectron Configurations. The experimental XAS spectra of the $[Fe(H_2O)_6]^{2+}$ and

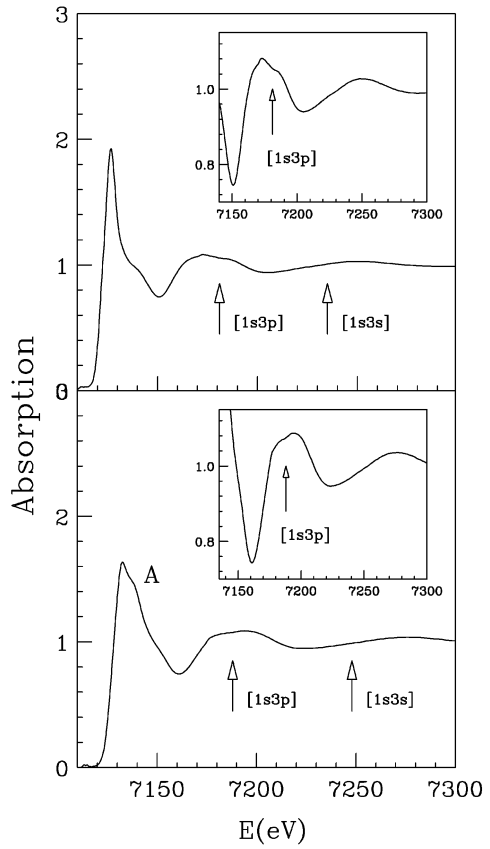

Figure 1. Normalized K-edge absorption spectra of Fe^{2+} (upper panel) and Fe^{3+} (lower panel) in water. Arrows refer to the thresholds for shake-up channels involving the additional excitation of the 3p and 3s electrons. The Fe^{3+} spectrum shows an additional structure (peak A), which is associated with the existence of an additional electronic configuration in the final state.

$[Fe(H_2O)_6]^{3+}$ complexes are shown in the upper and lower panels of Figure 1, respectively. Although these complexes are expected to have the same local geometry, their XANES spectra exhibit marked differences. The Fe^{3+} XAS cross section shows a broader main resonance peak, with a shoulder at about 6 eV from the first inflection point of the spectrum (feature A in Figure 1), compared to the Fe^{2+} case. In a recent work, it has been shown that this feature is not sensitive to pH changes and does not have its origin in a structural contribution.[10] All the attempts to fit the Fe^{3+} XANES experimental data by means of the MXAN procedure[24,25] produced unrealistic coordination geometries with a large mismatch between experimental and best-fit theoretical data. In particular, the one-electron approximation within the MS theory framework is not able to correctly reproduce the Fe^{3+} experimental data, and the low-energy features of the spectrum can be accounted for by considering a second excitation channel associated with an electronic final state configuration different than that of the fully relaxed one.[10]

Moreover, both the Fe^{2+} and Fe^{3+} water solution spectra show the presence of sizable features at about 7180 eV that alter the regularity of the first EXAFS oscillation, which is expected to have a simple sinusoidal behavior due to the octahedral symmetry of the first coordination sphere. Careful inspection of the magnified region of the spectra shown in the insets of Figure 1 reveals the existence of sharp features in the absorption coefficient around 7188 and 7181 eV for Fe^{2+} and Fe^{3+}, respectively. Note that, in the case of Fe^{3+}, this feature is broader than the corresponding structure of the Fe^{2+} spectrum, resembling the twin peak structure of the main transition edge. From these findings, it seems that, even if the 1s3p channel is very similar in the case of Fe^{2+} and Fe^{3+}, the atomic background for iron in different valence states is not completely transferable. In a previous investigation, it was shown that a unique atomic background can be defined for routine EXAFS analyses in the case of gaseous compounds of arsenic in different valence states.[26] Nevertheless, in the EXAFS analysis context, use of a fitting procedure that refines the parameters defining the atomic background overcomes this problem.

The energy positions of these anomalous structures are consistent with the energy onset of the 1s3p double-electron transition predicted by the Z+1 approximation. This approximation is the atomic limit of the more general MCMS theory. The channel assignments of Figure 1 have been obtained from the experimental data with the use of a proper background model as described in the previous section and confirmed by spin-polarized X-α self-consistent field (SCF) potential calculations. The identification of the 1s3s edge in the raw spectra is hampered by the superimposition of the oscillating structural contribution.

3.2. EXAFS Analysis of Fe^{2+} Aqueous Solution. To gain full understanding of the effect of double-electron excitations on the extraction of the structural parameters from the EXAFS data at the Fe K edge, we performed a thorough investigation of the $[Fe(H_2O)_6]^{2+}$ spectrum. As shown in the previous section, the Fe^{3+} water solution absorption cross section displays peculiar structures that reflect the presence of two configurations in the ground state which are not present in the case of Fe^{2+}. For this reason, the XAS analysis of the Fe^{3+} aqueous solution is expected to be affected by the presence of both multielectron excitations and multichannel processes, and a preliminary analysis of the Fe^{2+} data has been undertaken in an effort to shed light on the effect of double-electron excitations on the EXAFS results only.

For an aqueous system, in which there is a rather high degree of disorder, the XAFS oscillations are relatively weak and the opening of multielectron excitation channels can significantly distort the structural signal, especially for k smaller than 4 $Å^{-1}$. Yet, in the case of solutions and biological samples, where the available k range is usually narrow, it is important to extract the $\chi(k)$ to lower k values to maximize the spatial resolution, to better analyze asymmetric distribution functions, and to gain structural information on smaller atomic number backscatterers. In this case, it is crucial to efficiently remove multielectron excitations from the experimental spectra to obtain reliable structural information.

In the first step of the investigation, the low-energy region of the $[Fe(H_2O)_6]^{2+}$ spectrum comprising the double-electron channels was not considered, and the EXAFS data analysis was performed over the range $k = 5.4-12.5$ $Å^{-1}$. The $\chi(k)$ experimental signal was obtained by subtracting a smooth two-segmented spline function, and an octahedral geometry was considered for the first hydration shell.

The best-fit analysis of the Fe^{2+} water solution EXAFS spectrum is reported in the upper panel of Figure 2. The $\gamma^{(n)}$ signals are shown multiplied by k^2 in Figure 2 and in the other figures throughout the paper for better visualization. The first four curves from the top of the upper panel are the Fe−O and Fe−H first-shell $\gamma^{(2)}$ contributions and the MS signals associated with the 3 linear and 12 orthogonal O−Fe−O configurations. The reminder of the figure shows the total theoretical contribution compared with the experimental spectrum and the resulting residual. The agreement between the experimental data and the

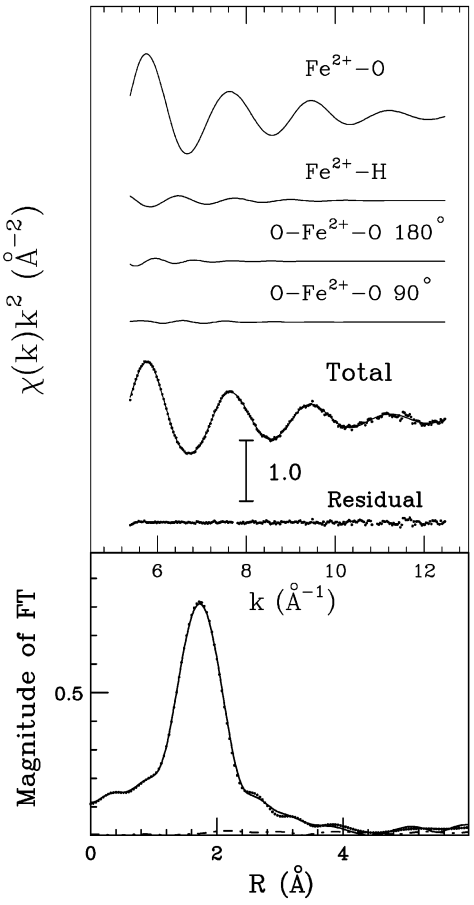

Figure 2. Upper panel: fit of the Fe^{2+} water solution EXAFS spectrum performed over the range $k = 5.4-12.5$ Å^{-1}. From the top to the bottom, the following curves are reported: the $Fe^{2+}-O$ two-body first-shell signal, the $Fe^{2+}-H$ two-body first-shell signal, the $O-Fe^{2+}-O$ linear and orthogonal three-body signals, the total theoretical signal (full line) compared with the experimental spectrum (dotted line), and the residual curve. Lower panel: non-phase-shift-corrected Fourier transforms of the experimental data (dotted line), of the total theoretical signal (full line), and of the residual curve (dashed−dotted line).

theoretical signal is excellent and the residual curve contains experimental noise only. The accuracy of the data analysis can also be appreciated by looking at the Fourier transform (FT) (non-phase-shift-corrected) of the experimental, theoretical, and residual signals shown in the lower panel of Figure 2.

As expected, the dominant contribution to the total XAFS curve is given by the Fe−O first-shell signal, but the Fe−H contribution is clearly detectable up to $k = 10$ Å^{-1}. Conversely, the amplitude of the MS signals associated with the O−Fe−O linear and rectangular configurations is quite low in this region of the spectrum. For this reason, the O−Fe−O three-body terms were kept fixed to an octahedral configuration, the bond−bond and bond−angle correlations have been assumed to be zero, and only the angle variances were refined. The best-fit values for the full set of structural parameters defining the Fe^{2+} first hydration sphere are listed in Table 1. Statistical errors were estimated by looking at the confidence intervals in the parameters' space. Standard deviations and correlation effects were obtained from correlation maps calculated for the parameters of each shell. The estimated statistical errors associated with the 95% confidence interval were obtained as described elsewhere.[15,27] The amplitude reduction factor, S_0^2, was found to be 0.94 ± 0.06, and the zero position of the theoretical scale was found at 0.3 ± 0.3 eV above the first inflection point of the spectrum.

It is worth stressing that the total number of parameters used in the fit is 11 (three parameters for each two-body signal, since the coordination numbers have been kept fixed, two angle variances associated with the three-body terms, plus three nonstructural parameters), and this value has to be compared to the number of independent data points, $N_I = (2\delta k \delta R/\pi) + 2 = 21$, for $\delta k = 7.1$ Å^{-1} and $\delta R = 4.4$ Å.[28] The independent data-to-parameter ratio shows that the fit is overdetermined, pointing to the reliability of the minimization. At the same time, we are sure that the structural parameters obtained from this analysis are not affected by the opening of the double-electron excitation channels, which occur in the energy range below 5 Å^{-1}.

In the second step of the investigation, the structural and nonstructural parameters derived from the short-range analysis were also used to calculate the $\chi(k)$ signal in the low-energy region where the 1s3s and 1s3p multielectron excitation edges are present. A conventional three-region polynomial spline was used to model the atomic background, while the theoretical signals were calculated starting from the parameters previously determined, without performing any minimization. The results of this procedure are shown in Figure 3. The agreement between the theoretical and the experimental signals is not satisfactory in the low-k region of the spectrum, and the residual curve shows a pattern with two step-shaped features around 3.9 and 5.3 Å^{-1}. The energy positions of these two structures (indicated in Figure 3 by arrows) correspond to the energy onsets of the 1s3p and 1s3s edges, respectively. As previously pointed out, even if the intensity of the double-electron channels is only a few percent of the single-electron transition, the amplitude and the frequency of the $\chi(k)$ first oscillation of the Fe^{2+} water solution spectrum are clearly distorted. As a consequence, the structural results obtained from a standard data analysis are expected to be affected by systematic errors if the low-k region is included.

A quantitative description of the intensity and shape of the multiexcitation edges was obtained using a proper model background, which reproduces the steps and changes of slope associated with the opening of double-electron channels. Additional least-squares fits were performed over the range $k = 3.1-12.5$ Å^{-1}, and the background model was refined together with the set of structural and nonstructural parameters mentioned

TABLE 1: Structural Parameters for Fe^{2+} and Fe^{3+} Water Solutions Obtained from the EXAFS Data Analysis

		N	R (Å)	R_m (Å)	σ^2 (Å^2)	β
$Fe^{2+}-O$	short-range analysis	6[a]	2.12(1)		0.008(1)	0.3(2)
	long-range analysis	6.0(2)	2.120(3)	2.100	0.0075(5)	0.3(1)
$Fe^{2+}-H$	short-range analysis	12[a]	2.85(5)		0.011(6)	0.5(3)
	long-range analysis	11.9(3)	2.84(2)	2.82	0.011(4)	0.5(2)
$Fe^{3+}-O$	one-electron analysis	6[a]	2.010(6)	2.000	0.0053(5)	0.5(2)
	MCMS analysis	6.0(2)	2.010(3)	2.000	0.0037(4)	0.5(2)
$Fe^{3+}-H$	one-electron analysis	12[a]	2.77(3)	2.72	0.0096(9)	0.8(3)
	MCMS analysis	12.0(3)	2.77(2)	2.72	0.0080(8)	0.8(3)

[a] Fixed parameter. The estimated standard deviations are given within parentheses for refined parameters.

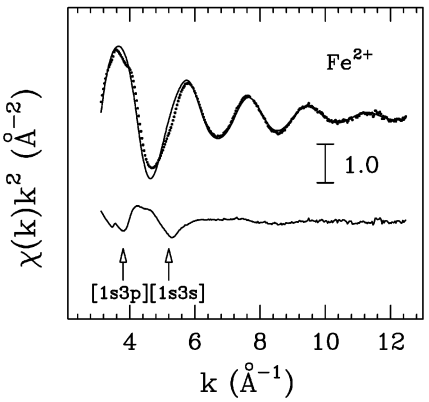

Figure 3. Comparison between the Fe^{2+} total theoretical curve (full line) and the $\chi(k)$ experimental spectrum (dotted line) extracted without the inclusion of the double-excitation edges. The residual curve shows the presence of two well-defined steps at about 3.9 and 5.3 $Å^{-1}$, which are associated with the KM_{23} and KM_1 double-excitation edges.

above. The parameters defining the 1s3p and 1s3s double-electron channels, obtained from the EXAFS minimization, are $E_d = 59$ and 108 eV, $\Delta E = 14$ and 80 eV, and $H = 6$ and 3% of the main transition edge intensity, respectively. To confirm these results and to provide a more accurate determination of the energy position of these multielectron excitation processes, we performed spin-polarized SCF calculations. These calculations were carried out by means of the standard SCF procedure, using an electronic high-spin configuration and a perfect octahedral geometry around the metal ion. The theoretical onset value of the 1s3p double-electron edge, obtained as the difference of the total energy between the $1sT^1_{1u}$ and the $\underline{1s}\ \underline{3p}\ T^1_{1u}{\uparrow}T^1_{1u}{\downarrow}$ electronic configurations was found to be 59.4 eV. As far as the 1s3s channel is concerned, the energy difference between the $1sT^1_{1u}$ and the $\underline{1s}\ \underline{3s}\ T^1_{1u}{\downarrow}A^1_{1g}{\downarrow}$ is about 91.2 eV. While the agreement between the experimental and calculated values is very good in the former case, the discrepancy in the latter case is on the order of 15%. This discrepancy could be due to the contribution of the shake-off channel, which shows a linear onset at the threshold with a large saturation range.

It is important to stress that even if the inclusion of each double-electron threshold implies the use of three additional adjustable parameters in the EXAFS data analysis, the extension of the available energy-range ($\delta k = 9.4$ $Å^{-1}$) greatly increases the number of independent experimental data points, and the N_I value supports the least-squares fitting procedure. Both the spline and the double-electron channel parameters have been found to be uncorrelated with the structural and nonstructural parameters obtained from the fitting procedure. In this case, the coordination number was also refined, and the statistical error on this parameter was evaluated. The best-fit analysis of the $[Fe(H_2O)_6]^{2+}$ spectrum is reported in Figure 4. After removal of multielectron excitations, there are significant improvements in the agreement between the experimental and theoretical curves in the k region below 5.4 $Å^{-1}$, and the anomalous structures in the residual curve are completely eliminated. The Fourier transform moduli of the EXAFS $\chi(k)k^2$ theoretical, experimental, and residual signals calculated over the k range 3.1−12.5 $Å^{-1}$ are shown in the lower panel of Figure 4. The FT spectra show a prominent first-shell peak, which is due to the Fe^{2+}−O first-shell distance. A second peak is present in the FT spectrum at about 2.4 Å, and it is associated with the hydrogen atoms, while the contribution at about 3.8 Å is due to the MS paths within the first hydration shell.

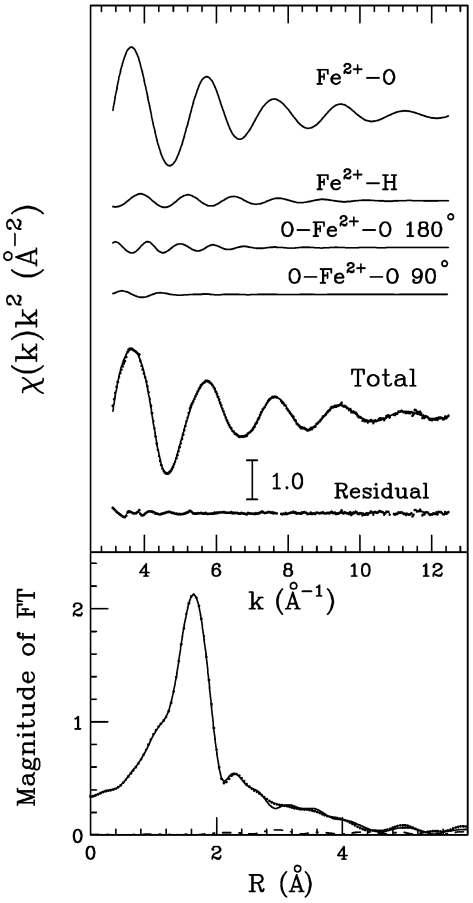

Figure 4. Upper panel: fit of the Fe^{2+} water solution EXAFS spectrum performed over the range $k = 3.1$−12.5 $Å^{-1}$. From the top to the bottom, the following curves are reported: the Fe^{2+}−O two-body first-shell signal, the Fe^{2+}−H two-body first-shell signal, the O−Fe^{2+}−O linear and orthogonal three-body signals, the total theoretical signal (full line) compared with the experimental spectrum (dotted line), and the residual curve. Lower panel: non-phase-shift-corrected Fourier transforms of the experimental data (dotted line), of the total theoretical signal (full line), and of the residual curve (dashed−dotted line).

First hydration shell structural parameters derived from this fitting procedure are presented in Table 1. These are not significantly different from the corresponding values obtained from the previous short-range analysis, even if the statistical errors are smaller. This finding enforces the reliability of the model atomic background used to extract the $\chi(k)$ signal. Note that the inclusion of the low-k region in the minimization allows the refinement of the structural parameters associated with the O−Fe−O three-body correlation functions. As already observed in the case of 3d transition metal ions in aqueous solutions, the amplitude of the MS paths within the first hydration shell is stronger for k values below 5 $Å^{-1}$, and the inclusion of this energy region is essential to gain information on the three-body distribution in solution.[16] Here, the average O−Fe−O angle value and the angle variance σ^2_θ were determined to be 178° and 4°^{2} for the linear three-body configuration, while the bond−bond correlation was found to be zero. Analysis of the MS signal associated with the 12 O−Fe−O rectangular configurations revealed an average angle value of 92°, with $\sigma^2_\theta = 6°^2$, while bond−bond and bond−angle correlations were found to be negligible. The nonstructural parameters were found to be equal to those previously determined, within the reported errors.

Finally, it would be of interest to observe the effect of the omission of the double-excitation contributions on the refined structural parameters. A fitting procedure was applied to the

EXAFS spectrum, extracted with a conventional smooth spline function over the k range 3.1−12.5 Å^{-1}. In this case, the agreement between the experimental and theoretical spectra is remarkably worse, and the fit index R_{sq} becomes 1 order of magnitude bigger than before. As far as the refined values are concerned, the most evident effect was observed for the Fe−O first-shell coordination number and the DW factor, while all the other parameters were found to be equal to the previous determination, within the reported errors. In particular, both the coordination number and the variance associated with the Fe−O two-body signal are underestimated by about 15% when double-excitation effects are not included. Moreover, the S_0^2 value obtained from this minimization was 0.94, a value only slightly smaller than the one obtained from the analysis accounting for double-electron excitation effects. This result was previously observed for other ions in water solution.[29]

3.3. EXAFS Analysis of the Fe^{3+} Aqueous Solution. The EXAFS analysis of the Fe^{3+} aqueous solution spectrum was performed along the line of the previous investigation. Least-squares fits of the experimental spectrum were carried out over the range k = 3.2−13.5 Å^{-1}, and double-electron excitation edges have been included in the atomic background, as previously described. The $\gamma^{(2)}$ and $\gamma^{(3)}$ signals associated with the Fe^{3+} first hydration shell were calculated within the usual one-electron scheme, and fitting procedures were applied to the whole set of structural and nonstructural parameters in order to improve, as far as possible, the agreement between the calculated signals and the experimental spectra. When the first-shell coordination number was allowed to vary in a wide range, the best-fit value was found to be 4.5. For this reason, the minimization was carried out using a fixed octahedral configuration of the water molecules around the Fe^{3+} ion, and the full set of refined structural parameters is listed in Table 1. As expected, both the Fe−O distance and the DW factor are lower for Fe^{3+} than for Fe^{2+}, due to the higher charge of the ion. The refined values of the O−Fe−O angles and angle variances were 178° and 5°^{2}, and 91° and 4°^{2} for the linear and rectangular configurations, respectively. The bond−bond and bond−angle correlations were found to be negligible, while E_0 and S_0^2 were 1.5 ± 0.4 eV from the first inflection point of the spectrum, and 0.97 ± 0.04, respectively.

Also, in this case, the inclusion of double-electron excitation edges in the atomic background gives rise to an excellent agreement between the experimental and theoretical spectra, in a wide k range. The parameters defining the 1s3p and 1s3s double-electron channels, obtained from the EXAFS minimization, are E_d = 60 and 110 eV, ΔE = 12 and 60 eV, and H = 8 and 2% of the main transition edge intensity, respectively. The results of the minimization are reported in Figure 5. Note that the hydrogen signal is clearly detectable up to k = 10 Å^{-1}, and its amplitude is slighter larger than that of the MS contributions. The magnitude of the FT of the experimental, theoretical, and residual signals is shown in the lower panel of Figure 5. In this case, the three frequency components from the Fe−O, Fe−H, and O−Fe−O configurations are clearly separated by the transformation.

EXAFS investigations on ionic solutions can provide not only reliable structural proprieties but also information on the ligand-exchange process in the first hydration shell. Sham was the first to point out that the ligand-exchange rate constant in water solution of 3d metal ions is closely related to the EXAFS Debye−Waller factor.[30] More recently Miyanaga et al.[31] showed that the σ^2 values do not reflect the real ligand exchange but rather the intrinsic character of the metal−oxygen bond. The

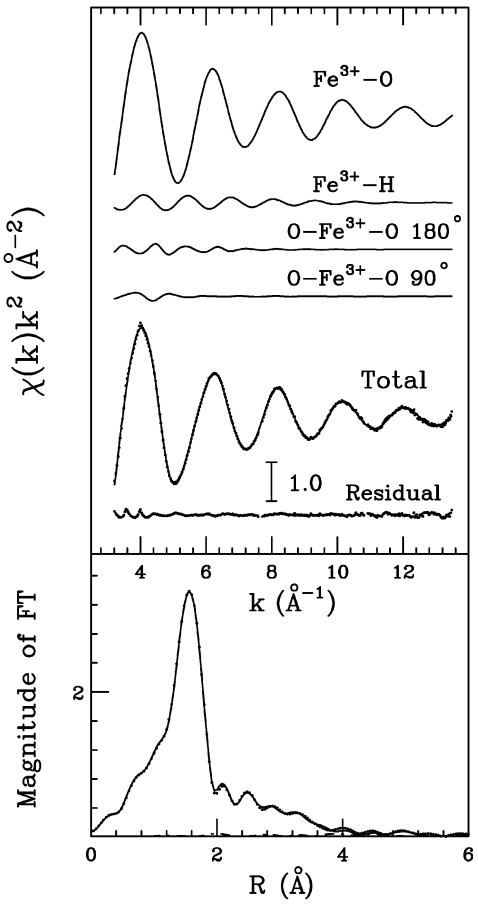

Figure 5. Upper panel: fit of the Fe^{3+} water solution EXAFS spectrum performed over the range k = 3.2−13.5 Å^{-1}. From the top to the bottom, the following curves are reported: the Fe^{3+}−O two-body first-shell signal, the Fe^{3+}−H two-body first-shell signal, the O−Fe^{3+}−O linear and orthogonal three-body signals, the total theoretical signal (full line) compared with the experimental spectrum (dotted line), and the residual curve. Lower panel: non-phase-shift-corrected Fourier transforms of the experimental data (dotted line), of the total theoretical signal (full line), and of the residual curve (dashed−dotted line).

rates of aqua metal ion substitution reactions, themselves, give little insight into the exchange mechanism, which is a subject of continuing debate and controversy. Today, there is a growing acceptance in the literature that the ligand-exchange reaction of 3d metal complexes is neither a dissociative nor an associative process, because the leaving or entering ligand always remains associated, to some degree, with the entire assemblage of hydrogen-bonded water molecules in the first and second hydration shells. A theoretical derivation of the correlation between DW factors and ligand-exchange rate constants k_1 was developed by Miyanaga et al.[31] under the assumptions that the reaction proceeds predominantly dissociatively and that the Morse-type interatomic potential is operative as reaction coordinate. According to this approach, the relation between σ^2 and log k_1 becomes:

$$(r^2/\sigma^2)^2 = K(\log A - \log k_1) \qquad (3)$$

where K is an arbitrary constant at a given temperature, r is the ion−nearest-neighbor distance, and A is a parameter linked to the maximum value of the ligand-exchange reaction rate pertaining to the zero activation energy. In Figure 6, the $(r^2/\sigma^2)^2$ values associated with the first-shell oxygen atoms of some 3d metal ions in aqueous solution are plotted against log k_1. The parameters for Fe^{2+} and Fe^{3+} are those determined from

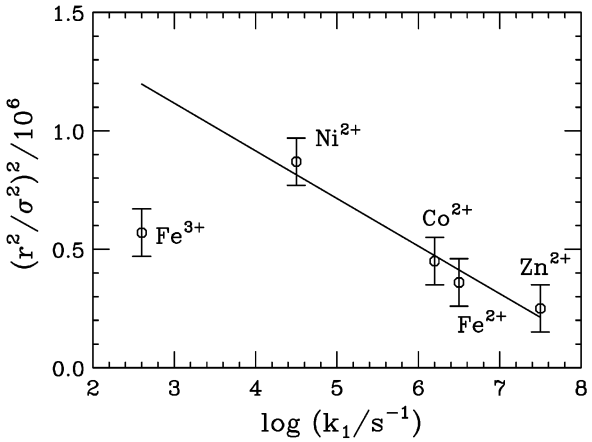

Figure 6. Relation between the EXAFS first hydration shell structural parameters of some metal ions (r is the first-shell distance and σ is the Debye−Waller factor) and log k_1 (k_1 is the ligand-exchange rate constant). The Fe^{3+} structural parameters refer to the EXAFS data analysis performed in the framework of the one-electron approximation.

the present EXAFS analyses, while for Ni^{2+}, Co^{2+}, and Zn^{2+}, r and σ^2 values are taken from ref 16. The ligand-exchange rate constant values are those reported in ref 31. All the EXAFS results are consistent with a linear dependence, as stated by eq 3, with the exception of the Fe^{3+} ion, which is out of the straight line by more than 3 times the value of the error bars. This is a clear indication that the $[Fe(H_2O)_6]^{3+}$ structural parameters obtained from the EXAFS data analysis performed in the framework of the one-electron approximation can be affected by systematic errors.

As previously mentioned, the $[Fe(H_2O)_6]^{3+}$ XANES spectrum was interpreted assuming the existence of two electronic configurations in the final state separated by an energy shift of about 6 eV.[10] According to the sudden limit of the MCMS theory, the total cross section can be written as the sum of two independent contributions, each of them arising from the electronic configurations present in the final state.[11] In particular, the total cross section $\sigma(\omega)$ can be written as

$$\sigma(\omega) = a^2_f\sigma_0(k_0) + b^2_f\sigma_1(k_1) \qquad (4)$$

where $\sigma_0(k_0)$ and $\sigma_1(k_1)$ are the partial cross sections corresponding to the fundamental and excited electronic configurations, with the wave vector given by $k_0^2 = \hbar\omega - I_c$ and $k_1^2 = \hbar\omega - I_c - \Delta E$. I_c is the photoemission binding energy and ΔE is the energy splitting between the two configurations in the final state. The coefficients a_f^2 and b_f^2 are the weights of the two channels, and, for the $[Fe(H_2O)_6]^{3+}$ complex, they were determined to be 0.72 and 0.28 for the excited and fundamental configurations in the final state, respectively.[10]

The presence of two channels with a comparable intensity is expected to affect the EXAFS structural determinations, especially concerning the structural parameters related to the intensity of the signal, and a deeper insight can be gained by using the multichannel theoretical approach previously described for the analysis of the EXAFS region. To this end, a further investigation of the $[Fe(H_2O)_6]^{3+}$ EXAFS spectrum was carried out accounting for the presence of two electronic configurations in the final state. In particular, using the same hydration geometry, we calculated two additional Fe−O and Fe−H $\gamma^{(2)}$ signals with a k scale shifted by 6 eV. A model EXAFS spectrum was generated by adding the Fe−water $\gamma^{(2)}$ contributions associated with the two channels, using weights of 0.72 and 0.28 for the excited and fundamental configurations, respectively. The total

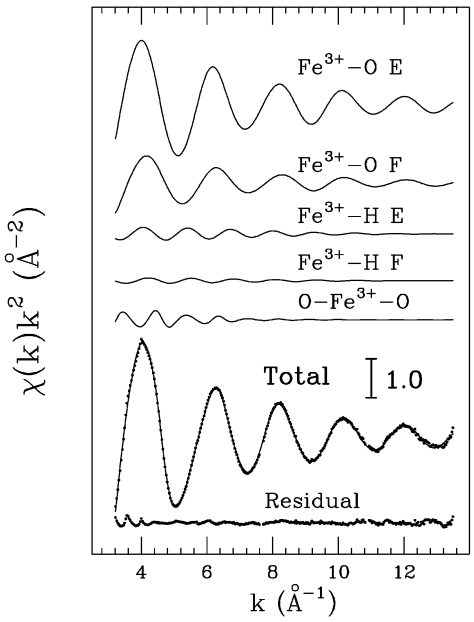

Figure 7. Fit of the Fe^{3+} water solution EXAFS spectrum performed over the range k = 3.2−13.5 Å^{-1} using the multichannel multiple-scattering theory. From the top to the bottom, the following curves are reported: the Fe^{3+}−O two-body first-shell signals associated with the excited (E) and fundamental (F) electronic configurations in the final state, the Fe^{3+}−H two-body first-shell signals associated with the excited (E) and fundamental (F) electronic configurations in the final state, the total O−Fe^{3+}−O three-body signal, the total theoretical signal (full line) compared with the experimental spectrum (dotted line), and the residual curve. The weights of the two channels are 0.72 and 0.28 for the excited and fundamental configurations, respectively.

TABLE 2: Fe−O and Fe−H Bond Distances for Fe^{2+} and Fe^{3+} Water Solutions

	method/reference[a]	Fe^{2+}	Fe^{3+}
R_{Fe-O}(Å)	XD, ND, EX/ref 10	2.10−2.28	1.99−2.05
	NDIS/ref 33,34	2.12	2.01
	MD(QM/MM)/ref 36	2.10	2.02
	EX/this work	2.100	2.000
R_{Fe-H}(Å)	NDIS/ref 33,34	2.75	2.68
	MD(QM/MM)/ref 36	2.83	2.72
	EX/this work	2.82	2.72

[a] The methods are abbreviated as follows: ND, neutron diffraction; XD, X-ray diffraction; EX, EXAFS; NDIS, neutron diffraction isotopic substitution; MD, molecular dynamics; and QM/MM, quantum-mechanical/molecular-mechanical.

$\chi(k)$ signal was refined against the experimental data by using a least-squares minimization procedure on a unique set of structural parameters. In this case, the first-shell coordination number was refined and a best-fit value of 6.0 ± 0.2 was found. Figure 7 shows the results of this analysis; the curves reported are the Fe^{3+}−O and the Fe^{3+}−H γ^2 theoretical signals associated with the excited and fundamental electronic configurations in the final state, the total MS contribution, their sum compared with the experimental data, and the residual. The agreement between the calculated and experimental spectra is very good and the R_{sq} value is equal to the one obtained from the one-electron analysis. The best-fit values are listed in Table 2. It is interesting to note that the structural parameters defining the frequency of the oscillation do not change with respect to the one-electron analysis, while a decrease of about 40 and 15% is obtained for the DW factors associated with the Fe−O and Fe−H signals.

The two-channel EXAFS data analysis of the Fe^{3+} spectrum gives rise to a lower DW factor, and the Fe^{3+}−O first-shell-

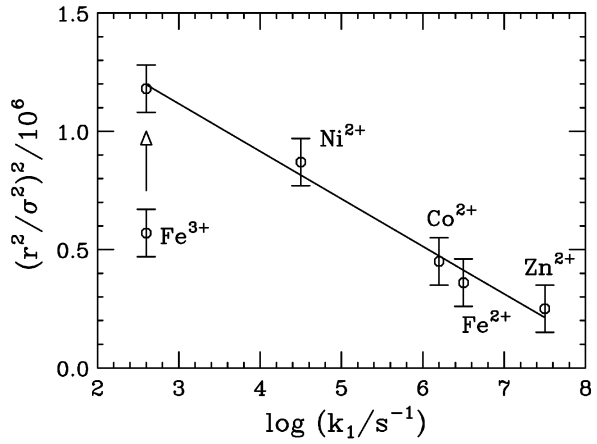

Figure 8. Relation between the EXAFS first hydration shell structural parameters of some metal ions (r is the first-shell distance and σ is the Debye−Waller factor) and log k_1 (k_1 is the ligand-exchange rate constant). The arrow shows the variation of the Fe^{3+} structural parameters obtained when the EXAFS data analysis is carried out in the framework of the multichannel multiple-scattering theory.

$(r^2/\sigma^2)^2$ value is now in excellent agreement with the linear dependence predicted by eq 3, as shown in Figure 8.

3.4. Structure of the Hydration Shells of Fe^{2+} and Fe^{3+}. Due to the important role of Fe^{2+} and Fe^{3+} in chemical and biological processes, several experimental and theoretical studies have been carried out on the hydration properties of these ions. X-ray diffraction (XRD) and neutron diffraction (ND) are the experimental techniques which have been most used for the determination of the coordination properties of ionic, aqueous solutions.[12] An important advantage of neutron diffraction over X-ray diffraction is the application of the isotopic substitution method (NDIS), which compares experimental data of samples with the same atomic composition, but different isotopes, for a particular element.[32,33] A peculiar and important characteristic of the ND technique is the ability to determine the ion−H (or ion−D) mean distance. Provided the ion−O distance is known, the orientation distribution of the hydrated water molecules can be obtained by neutron diffraction.[32]

All structural studies on the hydration properties of iron ions confirm the existence of well-defined octahedral complexes with Fe−O first-coordination peaks in the ranges 2.10−2.28 and 1.98−2.05 Å for Fe^{2+} and Fe^{3+}, respectively.[12,33] An outstanding experimental investigation was undertaken by Herdmann and Neilson on 1 *m* ferric and 1.52 M ferrous solutions,[34,35] using the NDIS technique, and the structural results obtained in this study are listed in Table 2. The distances between the water oxygens in the first hydration shell and the iron ions determined in our investigation are in good agreement with these NDIS results.

As previously mentioned, recent investigations have shown that the inclusion of hydrogen-scattering phenomena is essential to perform quantitative EXAFS analysis of aqueous solutions.[16,29] Here, the Fe−H contribution to the total $\chi(k)$ of aqueous Fe^{2+} and Fe^{3+} is clearly detectable up to $k = 10$ Å^{-1}, and the amplitude of the oscillations is about 15% of that of the oxygens. Proof of the importance of the hydrogen contribution was obtained by performing additional fitting procedures on the $[Fe(H_2O)_6]^{2+}$ spectrum, which did not include the hydrogen signal. The fitting procedures were applied both to the structural parameters associated with the Fe−O SS and MS signals and to the nonstructural and background parameters. It is important to outline that the E_0, the S_0^2, and the double-electron excitation values obtained from these minimizations

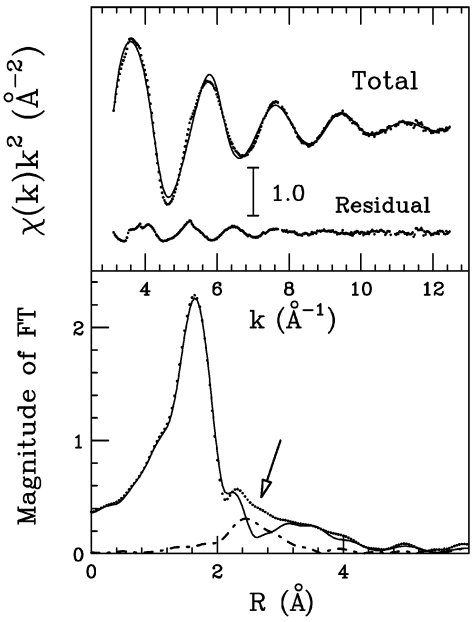

Figure 9. Upper panel: comparison between the Fe^{2+} EXAFS experimental spectrum (dotted line) and the theoretical signal not including the hydrogen contribution. Lower panel: non-phase-shift-corrected Fourier transforms of the experimental data (dotted line), of the total theoretical signal not including the hydrogen contribution (full line), and of the residual curve (dashed−dotted line). A peak at about 2.4 Å is clearly detectable in the residual signal and is associated with the hydrogen atoms.

were equal, within the reported errors, to those determined from the previous analysis including the hydrogen contribution. The results of this minimization are shown in the upper panel of Figure 9, where the total theoretical signal, including the Fe−O first-shell and the MS contributions, is compared with the experimental spectrum. The agreement between the experimental and theoretical signals is not particularly good, and the residual curve shows the presence of a leading frequency. The hydrogen contribution can also be clearly detected in the real-space $\bar{\chi}(R)$ data shown in the lower panel of Figure 9. When the hydrogen contribution is not included in the analysis, the theoretical curve does not reproduce the peak at about 2.4 Å, which is clearly associated with the hydrogen shell-distribution, as no other structural contributions are present in this distance range. On the other hand, the residual curve shows a well-defined peak at about 2.4 Å. Our estimates of the Fe−H distance are slighter longer than the values obtained from the NIDS investigations (see Table 2). It is important to stress that the R values reported in Table 1 are the average distances and not the positions of the maxima of the Fe−H peaks (R_m). In the presence of asymmetric distributions, R is longer than R_m, and the latter value should be compared with the NIDS experimental results. The Fe−H R_m values obtained from our analysis are 2.82 and 2.72 Å for Fe^{2+} and Fe^{3+}, respectively. These values correspond to a dipole orientation of the water molecules around the iron ions, while the mean ion−hydrogen distances obtained from the neutron diffraction studies imply a tilt angle for the ferrous and ferric ions of 32° and 20°, respectively.[34,35]

A similar result was obtained from a previous EXAFS investigation on a diluted Ni^{2+} aqueous solution, and, in this case, the EXAFS ion−H distance was slightly longer than that derived from neutron scattering.[16,36] This discrepancy could originate from the different concentration of the investigated samples, as the NDIS experiments are carried out on quite concentrated solutions (1 M is usually the lower limit). It is

reasonable to expect a concentration dependence of the hydration structure, and a tilted orientation of the water molecules could be favored by the formation of significant numbers of cation and anion ion pairs in the concentrated aqueous solutions. Proof of this hypothesis can be obtained by comparing our results with theoretical calculations. Recently, the hydration shell structures of Fe^{2+} and Fe^{3+} ions have been studied by combining ab initio quantum mechanical/molecular mechanical (QM/MM) molecular dynamics simulations.[37] The systems consisted of one ion plus 499 water molecules, thus reproducing an aqueous solution at infinite dilution. The characteristic values for the Fe−O and Fe−H model distribution functions obtained are listed in Table 2. In this case, there is a perfect agreement with our EXAFS determination, both for the Fe−O and Fe−H first-shell distributions. In this QM/MC molecular dynamics simulation, the angle ζ, defined by the Fe−O axis and the dipole vector of water, was used to characterize the orientation of water molecules. The distribution of cos ζ displays only peaks centered at −1.0 for both Fe^{2+} and Fe^{3+} (see Figure 2 of ref 37), pointing to a dipole configuration of the water molecules, in agreement with our results.

3.5. Discussion. Even if double-electron excitations and multielectron configurations in the final state are accounted for in the XAS data analysis using different approaches, these two phenomena originate from the same physical process with remarkably different intensities. In particular, the more the electronic configuration giving rise to many-body processes differs from the fully relaxed one, the lower the intensity of the many-body effect.

All the phenomena connected to the excitation dynamics, such as screening, polarization, relaxation, autoionization, etc., fall outside the realm of effective one-electron theory and must be treated on the basis of a general, many-body approach. The multichannel generalization of the MS theory is made including a channel index, which describes the final state of the excited $(N - 1)$ electron left behind by the photoelectron. In this way, one can take into account all possible outcomes of the photoemission process using a proper description of the $(N - 1)$ electrons. All the states having one or more electrons in the continuum, including both double photoionization processes and the existence of excited electrons in a valence state, can be treated on the same theoretical basis. Using this as a guide, it is possible to understand the effect of the many-body phenomena on the extraction of the structural information from the EXAFS experimental data and to quantify their effect on the derived structural parameters.

In this context, the analysis of the iron hydration complexes is quite informative; as in the case of Fe^{3+}, the multichannel processes arise both from double-electron excitations and from the presence of an additional electronic configuration in the final state, while the Fe^{2+} XAS spectrum is only affected by the opening of multielectron excitation channels. Investigation of these two systems allows one to gain interesting insights into the effect of both electronic dynamical processes on the extraction of the structural parameters from the EXAFS data. The omission of the 1s3p and 1s3s double-electron excitation channels has been found to have a rather small effect on the determination of the iron hydration complexes structural parameters, even if the quality of the fit gets remarkably worse. When multielectron photoexcitations are not accounted for, the DW factors and the coordination numbers are slightly underestimated. Conversely, the presence of two excitation channels in the low-energy region of the $[Fe(H_2O)_6]^{3+}$ spectrum hampers a reliable determination of the structural parameters when a one-electron scheme is used in the data analysis, despite the very good agreement between the theoretical and experimental spectra. In particular, the parameters related to the amplitude of the signal are affected by strong systematic errors, and when the EXAFS analysis is carried out on systems with unknown coordination geometries, it is not possible to determine the first-shell coordination numbers correctly. On the other hand, the presence of two electronic configurations in the final state makes it very difficult to extract structural information from the XANES spectrum. In this case, correct structural results can be obtained only from an EXAFS data analysis carried out on the basis of the MCMS theory.

4. Conclusions

A detailed investigation of the X-ray absorption spectra of Fe^{2+} and Fe^{3+} aqueous solutions has been performed, and, for the first time, the existence of double-electron excitation channels at the Fe K edge has been clearly shown. Anomalous features have been detected in the $[Fe(H_2O)_6]^{3+}$ XANES spectrum, which can be accounted for by considering two electronic configurations in the final state.

The influence of multielectronic configurations on the extraction of the structural parameters from the EXAFS spectra has been thoroughly investigated. Our analysis shows that the omission of double-electron excitation edges gives rise to slightly underestimated values of the first-shell coordination numbers and DW factors. Conversely, if the $[Fe(H_2O)_6]^{3+}$ EXAFS data analysis is carried out in the framework of the one-electron approximation, the refined structural parameters are affected by strong systematic errors; in this case, use of the MCMS theory is mandatory.

From our analysis, the short-range hydration structure of Fe^{2+} and Fe^{3+} has been determined with high accuracy. The two ions were found to be coordinated by six water molecules with iron−oxygen distances of 2.120 and 2.010 Å for Fe^{2+} and Fe^{3+}, respectively, in agreement with previous experimental and theoretical results. The EXAFS technique has been proven to provide reliable structural information on the Fe−H pair distribution functions. The Fe−H distances obtained from our analysis are in remarkably good agreement with ab initio QM/MM molecular dynamics determinations.

The results of the present investigation provide an invaluable insight and guideline for the correct analysis of XAS spectra at the Fe K edge.

Acknowledgment. We thank Prof. Bernd Michael Rode and Dr. Tawun vom Thailand for providing the Fe−H radial distribution function parameters obtained from their QM/MC MD simulations. We acknowledge the European Synchrotron Radiation Facility for provision of synchrotron radiation facilities, and we would like to thank Michael Borowski for assistance in using beamline BM29. This work was sponsored by the Italian National Research Council and by the Italian Ministry for the University and the Scientific and Technological Research (MURST).

References and Notes

(1) Rehr, J. J.; Albers, R. C. *Rev. Mod. Phys.* **2000**, *72*, 621.
(2) Joly, Y.; Cabaret, D.; Renevier, H.; Natoli, C. R. *Phys. Rev. Lett.* **1999**, *82*, 2398.
(3) Deslattes, D.; La Villa, R. E.; Cowan, P. L.; Hennis, A. *Phys. Rev. A: At., Mol., Opt. Phys.* **1983**, *27*, 923.
(4) Bernieri, E.; Burattini, E. *Phys. Rev. A: At., Mol., Opt. Phys.* **1987**, *35*, 3322.
(5) Ito, Y.; Nakamatsu, H.; Nukoyama, T.; Omote, K.; Yoshikado, S.; Takahashi, M.; Emura, S. *Phys. Rev. A: At., Mol., Opt. Phys.* **1992**, *46*, 6083.

(6) Arcon, I.; Kodre, A.; Štuhec, M.; Glavič-Cindro, D.; Drube, W. *Phys. Rev. A: At., Mol., Opt. Phys.* **1995**, *51*, 147.
(7) D'Angelo, P.; Di Cicco, A.; Filipponi, A.; Pavel, N. V. *Phys. Rev. A: At., Mol., Opt. Phys.* **1993**, *47*, 2055.
(8) Wu, Z.; Benfatto, M.; Natoli, C. R. *Phys. Rev. B: Condens. Matter Mater. Phys.* **1996**, *54*, 13409.
(9) Beaurepaire, E.; Kappler, J. P.; Malterre, D.; Krill, G. *Europhys. Lett.* **1988**, *5*, 369.
(10) Benfatto, M.; Solera, J. A.; García Ruiz, J.; Chaboy, J. *Chem. Phys.* **2002**, *282*, 441.
(11) Natoli, C. R.; Benfatto, M.; Brouder, C.; Ruiz Lopez, M. Z.; Foulis, D. L. *Phys. Rev. B: Condens. Matter Mater. Phys.* **1990**, *42*, 1944.
(12) Ohtaki, H.; Radnai, T. *Chem. Rev.* **1993**, *93*, 1157.
(13) Filipponi, A.; Borowski, M.; Bowron, D. T.; Ansell, S.; De Panfilis, S.; Di Cicco, A.; Itiè J.-P. *Rev. Sci. Instrum.* **2000**, *71*, 2422.
(14) Filipponi, A.; Di Cicco, A.; Natoli, C. R. *Phys. Rev. B: Condens. Matter Mater. Phys.* **1995**, *52*, 15122.
(15) Filipponi, A.; Di Cicco, A. *Phys. Rev. B: Condens. Matter Mater. Phys.* **1995**, *52*, 15135.
(16) D'Angelo, P.; Barone, V.; Chillemi, G.; Sanna, N.; Meyer-Klaucke, W.; Pavel, N. V. *J. Am. Chem. Soc.* **2002**, *124*, 1958.
(17) D'Angelo, P.; Di Nola, A.; Filipponi, A.; Pavel, N. V.; Roccatano, D. *J. Chem. Phys.* **1994**, *100*, 985.
(18) Filipponi, A. *J. Phys.: Condens. Matter* **1994**, *6*, 8415.
(19) Filipponi, A.; D'Angelo, P.; Pavel, N. V.; Di Cicco, A. *Chem. Phys. Lett.* **1994**, *225*, 150.
(20) Lindqvist-Reis, P.; Muñoz-Páez, A.; Díaz-Moreno, S.; Pattanaik, S.; Person, I.; Sandström, M. *Inorg. Chem.* **1998**, *37*, 6675.
(21) Hedin, L.; Lundqvist, B. I. *J. Phys. C: Solid State Phys.* **1971**, *4*, 2064.
(22) Krause, M. O.; Oliver, J. H. *J. Phys. Chem. Ref. Data* **1979**, *8*, 329.
(23) Burattini, E.; D'Angelo, P.; Di Cicco, A.; Filipponi, A.; Pavel, N. V. *J. Phys. Chem.* **1993**, *97*, 5486.
(24) Benfatto, M.; Della Longa, S. *J. Synchrotron Radiat.* **2001**, *8*, 1087.
(25) Benfatto, M.; Della Longa, S.; Natoli, C. R. *J. Synchrotron Radiat.* **2003**, *10*, 51.
(26) Kodre, A.; Prešeren, R.; Arčon, I.; Padežnik Gomilšek, J.; Borowski, M. *J. Synchrotron Radiat.* **2001**, *8*, 282.
(27) Filipponi, A. *J. Phys.: Condens. Matter* **1995**, *7*, 9343.
(28) Stern, E. A. *Phys. Rev. B: Condens. Matter Mater. Phys.* **1993**, *48*, 9825.
(29) D'Angelo, P.; Pavel, N. V.; Roccatano, D.; Nolting, H.-F. *Phys. Rev. B: Condens. Matter Mater. Phys.* **1996**, *54*, 12129.
(30) Sham, T. K. *Acc. Chem. Res.* **1986**, *19*, 99.
(31) Miyanaga, T.; Sakane, H.; Watanabe, I. *Bull. Chem. Soc. Jpn.* **1995**, *68*, 819.
(32) Neilson, G. W.; Ansell, S.; Wilson, J. *Z. Naturforsch. A: Phys. Sci.* **1994**, *50*, 247.
(33) Enderby, J. E. *Chem. Soc. Rev.* **1995**, *24*, 159.
(34) Herdmann, G. J.; Neilson, G. W. *J. Phys.: Condens. Matter* **1992**, *4*, 649.
(35) Herdmann, G. J.; Neilson, G. W. *J. Phys.: Condens. Matter* **1992**, *4*, 627.
(36) Powell, D. H.; Neilson, G. W. *J. Phys.: Condens Matter* **1990**, *2*, 3871.
(37) Remsungnen, T.; Rode, B. M. *J. Phys. Chem. A* **2003**, *107*, 2324.